

The quantum annealing gap and quench dynamics in the exact cover problem

Bernhard Irsigler and Tobias Grass

ICFO-Institut de Ciencies Fotoniques, The Barcelona Institute of Science and Technology, 08860 Castelldefels (Barcelona), Spain

Quenching and annealing are extreme opposites in the time evolution of a quantum system: Annealing explores equilibrium phases of a Hamiltonian with slowly changing parameters and can be exploited as a tool for solving complex optimization problems. In contrast, quenches are sudden changes of the Hamiltonian, producing a non-equilibrium situation. Here, we investigate the relation between the two cases. Specifically, we show that the minimum of the annealing gap, which is an important bottleneck of quantum annealing algorithms, can be revealed from a dynamical quench parameter which describes the dynamical quantum state after the quench. Combined with statistical tools including the training of a neural network, the relation between quench and annealing dynamics can be exploited to reproduce the full functional behavior of the annealing gap from the quench data. We show that the partial or full knowledge about the annealing gap which can be gained in this way can be used to design optimized quantum annealing protocols with a practical time-to-solution benefit. Our results are obtained from simulating random Ising Hamiltonians, representing hard-to-solve instances of the exact cover problem.

1 Introduction

Quantum annealers [1–3] are an emerging technology which combine features from analog quantum simulators [4–6] and digital, gate-based quantum computers [7]. Like in quantum simulators, the engineering of a Hamiltonian is the working scheme in quantum annealers, but these devices feature also microscopic design opportunities which allows one to choose a Hamiltonian

such that its ground state solves a specific instance of a general computational problem. For example, any NP-hard optimization problem can be mapped onto an Ising spin model with tunable couplings [8]. Together with a transverse field term producing quantum fluctuations, this Ising Hamiltonian is the central element of existing quantum annealers, specifically the commercial D-wave device [9], as well as in atomic annealing architectures [10–14] which have been proposed. In the absence of decoherence, the quantum annealing algorithm tries to find the ground state of the model through an adiabatic dynamical process, i.e. adiabatic state preparation or adiabatic quantum computing [15]. In the presence of decoherence, the dynamical process to find the ground state resembles more a conventional thermal cooling process, yet with a quantum feature which provides control over quantum fluctuations [16, 17]. In both cases, the dynamical evolution encounters configurations in which the energy gap above the instantaneous ground state becomes exponentially small [18–22], and this becomes the bottleneck of the quantum annealing method. Therefore, different strategies to avoid small energy gaps have been reported, including inhomogeneous transverse fields [23–26], non-stoquastic driver Hamiltonians [27–31], reverse or biased annealing [32–35], as well as combinations thereof [36]. There are also different hybrid algorithms which may avoid the annealing bottleneck [37–40].

A simple strategy which can improve the fidelity of the quantum annealing method is the deceleration of the annealing process around the minimal gap. In this way, the efficiency of the adiabatic Grover algorithm could be improved from $T \sim \mathcal{N}$ to $T \sim \sqrt{\mathcal{N}}$ [41], where T is the annealing time and \mathcal{N} is the Hilbert space dimension of the system. This remarkable result, however, relies on the analytical accessibility of the prob-

lem. Strikingly, also in the case of quantum annealing far away from the adiabatic regime, experiments on the D-wave device have shown that pausing the evolution near the minimal gap is beneficial for the annealing fidelity [42]. This experimental observation has theoretically been explained in Ref. [43], attributing the improvement of the quantum annealing to thermalization. No clear time-to-solution improvement from pausing, however, has been found yet [43]. Nevertheless, the pausing feature suggests that, in both adiabatic and non-adiabatic scenarios, knowledge of the instantaneous energy gap above the ground state could help to speed-up the annealing process. In the present work, we investigate how such knowledge can be obtained through simple quench experiments, and be refined through machine-learning techniques.

Although adiabatic evolution and quenching are two opposite extremes with a clear discrepancy in the time-dependence of the field, relations between the two approaches have been studied [44, 45]. A physical phenomenon which can occur after a quantum quench is the so-called dynamical quantum phase transition, which may be manifested from the behavior of an order parameter after the quench [46, 47]. Specifically, it has been shown for the long-times dynamics in long-range transverse-field Ising models that the non-zero magnetization of a system which is initially in the ferromagnetic phase averages to zero during the evolution after quenching with a sufficiently strong transverse field [48–53]. This phenomenon has also been experimentally observed in a trapped-ion experiment [54].

The present manuscript considers a somewhat similar scenario, but with some "randomness" in the Ising couplings. In the absence of a transverse field, this "randomness" makes the system behave rather like a spin glass than a ferromagnet. In fact, we will define the "random" couplings through randomly generated (but well characterized) instances of an NP-hard optimization problem, specifically the exact cover problem which is frequently studied in the context quantum annealing, see Refs. [15, 21, 35]. Analyzing the dynamical behavior of different order parameters, related to either the local magnetization of the system in the glassy ground state or to the paramagnetic order in a strong transverse field, we first determine a "critical" field strength in the

quench dynamics. Assuming that the dynamical behavior in the quench dynamics is related to the equilibrium paramagnetic and glassy states, we establish through numerical simulations that the annealing bottleneck coincides with the critical field value of the quench. We then show that this connection between quench and annealing dynamics can be used to design quantum annealing protocols with a significant fidelity enhancement, as compared to the standard annealing protocol with a constant ramp speed. Importantly, the proposed method to improve the annealing result does not rely on any previous knowledge of the problem instance, but only on information which can be collected through a few quench experiments.

In a second step, we explore how the connection between quench and annealing dynamics can be extended beyond the matching at only one critical field strength. To this end, we have trained a neural network which maps the order parameter as a function of the quench field to the energy gap during the annealing process. We note that, in comparison to reinforcement learning strategies which in the past have been applied to problems from optimal control [55] and quantum annealing [56], our approach has only a small amount of training requirements, as our method is based on supervised training of only a single-layer network. Nevertheless, after this training process, it becomes possible to fully and almost exactly reproduce from the quench data the annealing gap as a function of the transverse field strength. With this information, it then becomes possible to adjust the instantaneous ramp speed of the annealing protocol. Not surprisingly, this yields a further fidelity improvement, as compared to our first method which had not required any network training.

Our paper is organized in three Sections: In Sec. II, we describe the studied computational problem, and define the annealing gap, as well as the order parameters in the quench dynamics. We distinguish two types of quenches: switching the transverse field on or off. In Sec. III, we present the results which in subsection (A) consists of a relation between quenched order parameters and annealing gap, and in subsection (B) of an application of this connection to the quantum annealing protocol. In both subsections, we further distinguish between (1.) the connection

which can immediately be made at the critical field strength, and (2.) the connection at arbitrary field strengths, obtained after training a neural network. Finally, in Sec. IV, we summarize our results, and briefly discuss the technological advances associated with our results.

2 Definitions

2.1 Model

We define the annealing Hamiltonian as

$$\hat{H}[h(t)] = (1 - h(t))\hat{H}_p + h(t)\hat{H}_q, \quad (1)$$

herein, we introduced the problem Hamiltonian \hat{H}_p , the fluctuation Hamiltonian \hat{H}_q , and the time-dependent field $h(t)$. We focus on the exact cover (EC) problem to be embedded in the problem Hamiltonian. In the language of spins, the EC problem is described by a set of clauses C containing M tuples of randomly selected spins, each point either up or down. In our case, we focus on the EC3 problem, i.e., those tuples will be triples. In EC3, a clause is fulfilled if exactly two of the three spins point up while one of them points down. Since, different clauses can share the same spins, the problem can become hard to solve. It is assumed that for $M \approx N$ the problem is hard, where N is the number of spins in the system. In this regime, many instances have exactly one solution, dubbed as unique satisfying assignment. We focus solely on those instances. The classical EC3 problem can be expressed in a Hamiltonian in the following way:

$$\hat{H}_p = J \sum_{(i,j,k) \in C} (\hat{\sigma}_i^z + \hat{\sigma}_j^z + \hat{\sigma}_k^z - 1)^2, \quad (2)$$

where J is the energy scale. The set C contains M random triples, dubbed clauses, such that

$$C = \{(i, j, k) : i \neq j \neq k \in [1, 2, \dots, N]\}, \quad (3)$$

where N is the number of spins in the system. If a spin configuration satisfies all clauses in C , its energy associated with Eq. (2) is zero. On the other hand, every clause which is not fulfilled by a spin configuration leads to an energy cost of at least $4J$. Therefore, for the instances of C which have unique satisfying assignment, there is one zero-energy state, being the non-degenerate ground state of \hat{H}_p .

For the fluctuation Hamiltonian we employ a transverse spin term as

$$\hat{H}_q = J \sum_{i=1}^N \hat{\sigma}_i^x. \quad (4)$$

Here, we define the fluctuation Hamiltonian using the same energy scale J as in the problem Hamiltonian, but in the annealing Hamiltonian, as described by Eq. (1), the dimensionless function $h(t)$ controls the energetic weight of \hat{H}_q and \hat{H}_p .

Throughout this manuscript, we make use of the quspin package for the exact diagonalization, quenches and time evolutions [57, 58].

2.2 Annealing gap

We define the annealing gap $\Delta(h)$ as the energy gap between the two lowest energy levels $E_n(h)$ of the Hamiltonian in Eq. (1) rescaled by the bandwidth $W(h)$ for time-independent $h(t) = h$:

$$\Delta(h) = \frac{E_1(h) - E_0(h)}{W(h)}, \quad (5)$$

$$W(h) = E_{2N}(h) - E_0(h).$$

We compute the minimal annealing gap h_c^Δ by determining numerically the global minimum of the gap of the annealing Hamiltonian in Eq. (1) for $0 < h < 1$ being time-independent. The result is shown in Fig. 1 as a probability distribution. We observe that the probability distributions become broader with increasing N as more complex configurations of the problem Hamiltonian can emerge.

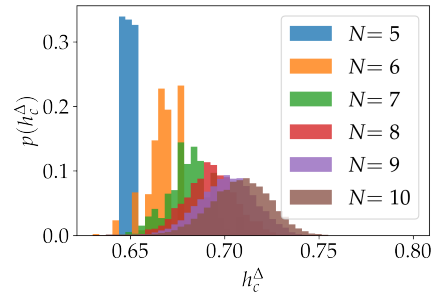


Figure 1: Probability distribution of the minimal annealing gap h_c^Δ for different system sizes N .

2.3 Quench dynamics

The dynamical quantum phase transition is achieved through a sudden quench of the field

$h(t)$ in the Hamiltonian in Eq. (1) in the thermodynamic limit. As we consider finite systems, we will define dynamical quench parameters (DQP) analogous to order parameters in the thermodynamic limit in order to distinguish between different states within the quench dynamics. We differentiate between the instantaneous ground states $|\psi_h\rangle$, which are eigenstates of the Hamiltonian in Eq. (1), and the time-evolved states $|\psi_h(t)\rangle = \hat{U}(t, 0)|\psi_h\rangle$. Here,

$$\hat{U}(t, 0) = \mathcal{T} \exp \left[-i \int_0^t \hat{H}(t') dt' \right] \quad (6)$$

is the time-evolution operator. Herein, \mathcal{T} is the time-ordering operator and $\hbar = 1$. In the following, we treat two different kinds of quenches associated with different initial states and different DQPs.

2.3.1 "switch on"

This procedure is similar to the one used in Ref. [51] for treating the clean Ising model. The initial state is the groundstate of $\hat{H}[h = 0]$ which is then quenched to the final field h_f with finite value $0 < h_f \leq 1$. The associated observable is

$$G(h_f, t) = \frac{1}{N} \sum_{i=1}^N \langle \psi_0 | \sigma_i^z | \psi_0 \rangle \langle \psi_{h_f}(t) | \hat{\sigma}_i^z | \psi_{h_f}(t) \rangle. \quad (7)$$

We note that for $t = 0$, $|\psi_{h_f}(t)\rangle = |\psi_0\rangle$ and therefore $G(h_f, 0) = 1$. The corresponding DQP is defined as

$$G(h_f) = \lim_{\tau \rightarrow \infty} \frac{1}{\tau} \int_0^\tau G(h_f, t) dt. \quad (8)$$

2.3.2 "switch off"

This procedure is more relevant for quantum annealing since here the fluctuation field is initially maximal, $h = 1$, and is then quenched to $0 \leq h_f < 1$. Also, it does not require any prior language about the groundstate of the problem Hamiltonian $|\psi_0\rangle$. For the "switch off" procedure the associated observable is defined as

$$X(h_f, t) = \frac{1}{N} \sum_{i=1}^N \langle \psi_h(t) | \hat{\sigma}_i^x | \psi_h(t) \rangle \quad (9)$$

As in the example above, for $t = 0$, $|\psi_{h_f}(t)\rangle = |\psi_1\rangle$ and therefore $X(h_f, 0) = 1$. The corresponding DQP is defined as

$$X(h_f) = \lim_{\tau \rightarrow \infty} \frac{1}{\tau} \int_0^\tau X(h_f, t) dt. \quad (10)$$

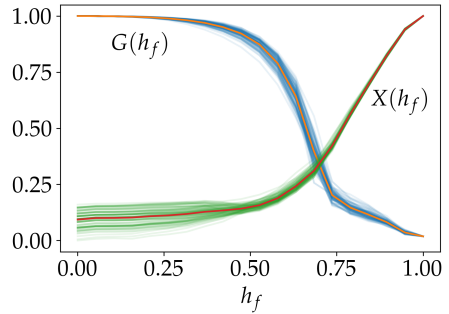


Figure 2: DQPs as a function of the quench field h_f for 100 different instances of the problem Hamiltonian in Eq. (2). Thick lines correspond to the respective averages.

3 Results

Our results are twofold. On the one hand, we show the correlation between the minimal annealing gap and the DQP which connects two both dynamical but very different approaches. On the other hand, we use the possibility to predict the annealing gap from the result of quench experiments to gain a time-to-solution improvement over the standard annealing procedure.

3.1 Relation between annealing gap and quench dynamics

While annealing and quenching are at the opposite sides in terms of time dependence, they may actually reveal the same information about a quantum state. In the following, we want to investigate whether the annealing gap can be estimated from the information drawn from the DQP.

3.1.1 Critical field from linear regression

To this end, we employ a multivariate linear regression. The DQP in Fig. 2 are plotted on a discretized one-dimensional grid for h_f , with 20 points i.e., h_f^n for $n = 1, 2, \dots, 20$. The values the DQP assumes at these points, e.g., $G(h_f^n)$, are then used as estimators in the multivariate regression. The predictions from the estimators $G(h_f^n)$ are presented in Fig. 3(a) and those of the estimators $X(h_f^n)$ are presented in Fig. 3(b). The predictions are both plotted versus the true values of the minimal gap.

We introduce the Pearson's r as a measure for the linear correlation between two random vari-

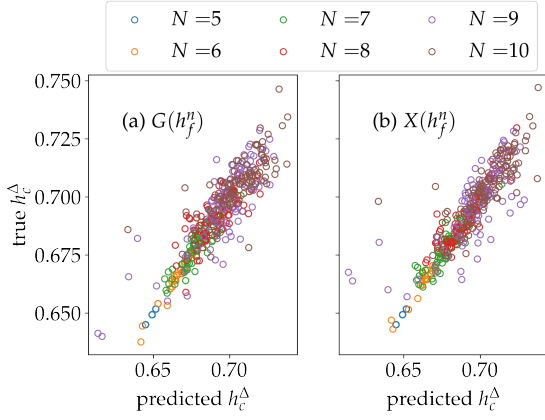


Figure 3: Predicted values for the field of the minimal gap h_c^Δ through multivariate regression of the (a) $G(h_f^n)$ and (b) $X(h_f^n)$ estimators, respectively, versus true values of h_c^Δ .

ables x and y :

$$r = \frac{\langle (x - \langle x \rangle)(y - \langle y \rangle) \rangle}{\sqrt{\langle (x - \langle x \rangle)^2 \rangle} \sqrt{\langle (y - \langle y \rangle)^2 \rangle}} \quad (11)$$

In particular, we want to quantify how well our predictive methods work by interpreting x as the true values and y as the predicted values. In Fig. 4, we show the Pearson's r quantifying the predictive power of the $G(h_f^n)$ and $X(h_f^n)$ estimators as a function of the number of spins in the system. While decreasing with the system size, we still observe strong correlation between the predicted and the true minimal gap. We conclude that the DQP contains information about the quantum state change during the annealing process.

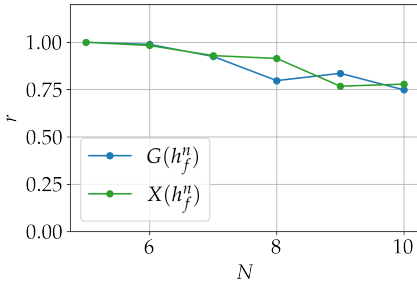


Figure 4: The Pearson's r as a function of the system size N for both quench approaches.

3.1.2 Full gap function from neural network

In the previous section we have shown that the value for the critical field at the minimal gap h_c^Δ can be obtained from the DQP as a function of

the field h . In the present section, we employ modern machine-learning techniques [59] to acquire not only the value of h_c^Δ but the full function $\Delta(h)$ in the entire regime $0 < h < 1$.

Compared to conventional algorithms, neural networks work best for a large amount of data. Therefore, we restrict ourselves to the system size of $N = 7$ and create 5000 random instances of the Hamiltonian in Eq. (2). We then compute $\Delta(h)$ as well as $X(h_f)$, see Eqs. (5) and (10), respectively. Both functions are evaluated on an equidistant grid of 128 points. Note that it is not required by the algorithm that both functions are discretized by the same number of data points.

We make use of the established high-level package Keras [60] in order to construct a simple neural network with one single dense layer exhibiting a linear activation function. We use the mean square error as the loss function, a batch size of 64 and the ADAM optimizer [59]. Out of the full data set of 5000 instances, we use 4000 as the train/validation data set and 1000 as the test data set. The validation data set is another split of 20% of the 4000 instances.

We show the training of the neural network in Fig. 5. After 600 epochs, we achieve a loss of $\sim 10^{-6}$. In order to make sure that there is no overfitting occurring during the training, we plot the loss for the validation set, i.e., the loss on the data the neural network has not seen before. Since validation loss behaves exactly like the loss function itself, we can be certain that there is no overfitting happening. The only free parameter in our neural network is the learning rate which enters in the optimizer. We have found through a grid search that $5.5 \cdot 10^{-4}$ leads to the lowest loss.

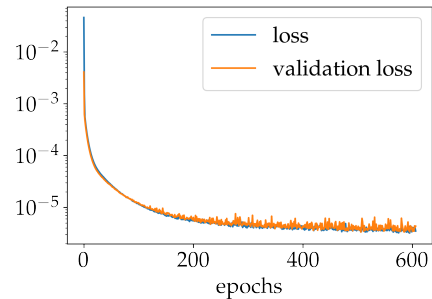


Figure 5: Training of the neural network: evolution of the loss and the validation loss over the episodes. We plot the validation loss in order to rule out possible overfitting.

Finally, we plot some instances for the gap

function as predicted by the trained neural network from the test data set in Fig. 6. We compare these predictions with the true gap functions out of the test set shown as dashed curves in Fig. 6.

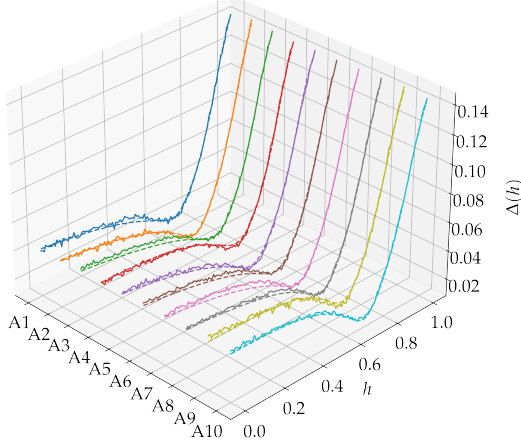


Figure 6: Predictions for the gap of the test data as solid lines and the respective true gap functions as dashed lines. The different instances are labeled by A1 to A10. The diagonal of the respective Hamiltonian \hat{H}_p , see Eq. (2), is provided in the supplemental material.

3.2 Time-to-solution improvement for annealing

In this section, we want to draw a technical benefit out of the knowledge of the annealing gap. Specifically, we design annealing protocols with non-linear time dependencies which, at a fixed annealing time, lead to a better final fidelity than the protocol with homogeneous ramp speed. For the construction of these inhomogeneous protocols, we first restrict ourselves to exploiting the correlation between minimal gap and DQP. As shown in the previous Section, this information is readily obtained from quench experiments. In a second step, we will further refine the annealing strategy by exploiting the full knowledge of the annealing gap, which we have shown to be accessible through a combination of quench data and machine learning.

3.2.1 Protocols with slow-down at critical field strength

We perform calculations for the full time evolution in order to simulate the annealing procedure at finite times. In this way, we compare annealing protocols which have a linear ramp, and an

nealing protocols which are piecewise accelerated. The linear ramp has the following form

$$h_{\text{lin}}(t) = 1 - \frac{t}{T}, \quad (12)$$

where T is the duration of the annealing procedure. The second protocol is a combination of two quadratic functions

$$h_{\text{quad}}(t, h_c) = \begin{cases} 1 + b_1 t + c_1 t^2, & \text{if } t < t_c \\ a_2 + b_2 t + c_2 t^2, & \text{if } t \geq t_c. \end{cases} \quad (13)$$

Here, we have introduced a critical field h_c where the annealing protocol should slow down. We assume that h_c is reached at time $t_c = (1 - h_c)T$ where the annealing gap might be small. Later, we will compare different values for h_c . The coefficients in Eq. (13) are determined by implying a smooth function $h_{\text{quad}}(t, t_c)$ and a vanishing velocity at the critical point in time $\partial_t h_{\text{quad}}(t, t_c)|_{t=t_c} = 0$.

We define the fidelity as the overlap of the instantaneous ground state and the time-evolved ground state at the end of the annealing procedure, $|\langle \psi_0 | \psi_1(T) \rangle|$. There are different possibilities to determine the critical field h_c . The most simple one is to set it to a constant, e.g., 0.5. This will serve as a reference. Moreover, one can determine instance-specific critical fields h_c . In that case, the minimal annealing gap h_c^Δ is a possible candidate. This quantity, however, is not accessible a priori from an experimental point of view. Therefore, we also use critical fields which are determined from the DQP and thus accessible through quench experiments. We define

$$h_c^G, \text{ where } G(h_f = h_c^G) = 0.5 \quad (14)$$

$$h_c^X, \text{ where } X(h_f = h_c^X) = 0.5 \quad (15)$$

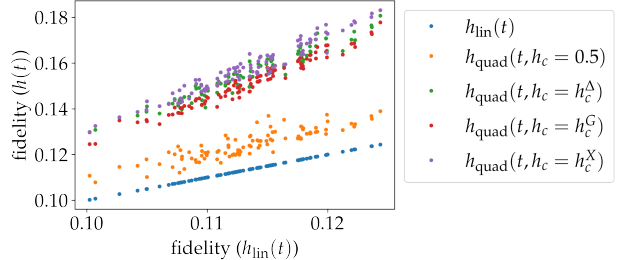


Figure 7: Fidelity for five different annealing protocols for $N = 10$ and $T = 1$, see Eqs. (12) and (13).

In Fig. 7, we show exemplarily the results for the fidelity of four different quadratic anneal-

ing protocols compared to the fidelity of the linear protocol $h_{\text{lin}}(t)$ defined in Eq. (12). While one quadratic protocol is chosen independent of the respective instance of the problem Hamiltonian, the other quadratic protocols depend on an instance-specific critical field value as an input parameter. We observe that these last three protocols yield a significant improvement with respect to the instance-independent protocol.

We are now interested in the scaling of these protocols with respect to the number of spins in the system. The average fidelity as a function of the number of spins is shown in Fig. 8 for the five different protocols. In order to quantify the time-

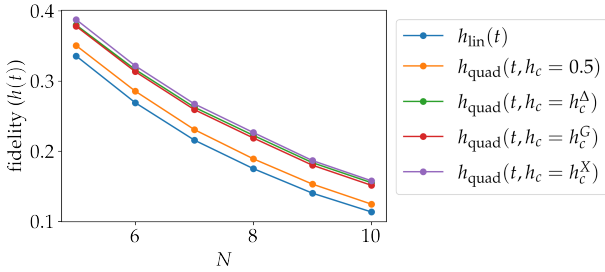


Figure 8: Scaling of the average fidelity as a function of the number of spins in the system for $T = 1$.

to-solution improvement we compute the annealing time evolution for different annealing times T . We then determine the isobaric lines of constant average fidelity in order to find the scaling of T as a function of N . Those isobaric lines are shown in Fig. 9 for the best and the worst protocol. We observe that both scale approximately linearly, $T \sim N$, at least in the regime $5 \leq N \leq 10$. However, the quadratic protocol which uses the critical field h_c^X certainly exhibits a smaller prefactor for the scaling.

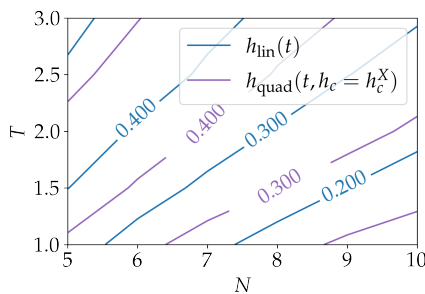


Figure 9: Scaling of the worst and the best annealing protocol shown through the isobaric lines of constant average fidelity.

3.2.2 Protocols utilizing the full gap function

In the previous section, we have observed that the knowledge of a critical field obtained from, e.g., the DQP, can improve the time-to-solution of the annealing process. In this section, we will investigate whether we can improve this even further, assuming we have knowledge about the full gap function. As shown in Sec. 3.1.2, the combination of quench data and neural network training might be an accurate source of this information.

Inspired by the adiabatic theorem, we assume that the optimal protocol should scale with the size of the gap

$$\frac{dh(t, \alpha)}{dt} \propto |E_1(t) - E_0(t)|^\alpha. \quad (16)$$

Here, we have introduced a free parameter α which in the most standard version of the adiabatic theorem [2] would be $\alpha = 2$. We note that the adiabatic theorem contains a matrix element of the Hamiltonian which couples the two states of interest. As it has been done in Ref. [41], we approximate this matrix element by the time derivative of the protocol $h(t, \alpha)$. Furthermore, we note that Eq. (16) considers only transitions between the energetically lowest two states. In fact, our systems of interest have 2^N states, and generally all transitions depleting the groundstate contribute to the loss of annealing fidelity. Thus, Eq. (16) is certainly to be understood as an approximation. This also means that there might not be a universal α which is optimal for all the spin glass instances we investigate.

We now use Eq. (16) in order to find an optimized annealing protocol. In a discretized form, this means

$$\Delta t_i = \frac{|E_1(t_i) - E_0(t_i)|^{-\alpha}}{\sum_j |E_1(t_j) - E_0(t_j)|^{-\alpha}} T, \quad (17)$$

where we have introduced the discretized time $t_{i+1} = t_i + \Delta t_i$. Also note that this protocol is normalized to the duration of the annealing process $\sum_i \Delta t_i = T$. For $\alpha = 0$, the protocol becomes the standard linear protocol as Eq. (12).

In Fig. 10, we show annealing protocols $h(t, \alpha)$ constructed according to Eq. (17) for different values of α as a function of time. We also show the evolution of the fidelity with respect to time. First, the protocols $h(t, \alpha)$ with finite α improve the fidelity at the end of the annealing, as compared to the linear protocol $\alpha = 0$. Secondly, we

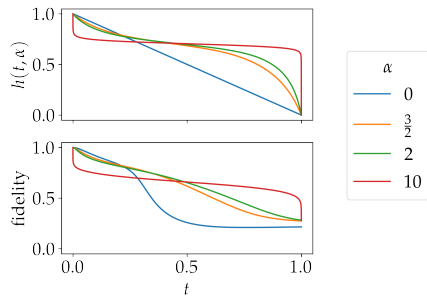


Figure 10: Full gap annealing protocols according to Eq. (17) for different values of α and a single Hamiltonian instance. The diagonal of the respective Hamiltonian \hat{H}_p , see Eq. (2), is provided in the supplemental material with the label B1.

observe that the fidelity for larger values of α is similar at $t = T$. In Fig. 11, we show the fidelity at the end of the annealing process as a function of α for a single instance. We observe that the maximum is achieved for $\alpha = 3$. As we have mentioned before, this value is not universal and differs from instance to instance. We also include in Fig. 11 the values for the fidelity of the quadratic protocols investigated in the section before. We conclude that knowledge of the full gap function can indeed lead to a further improvement of the annealing process.

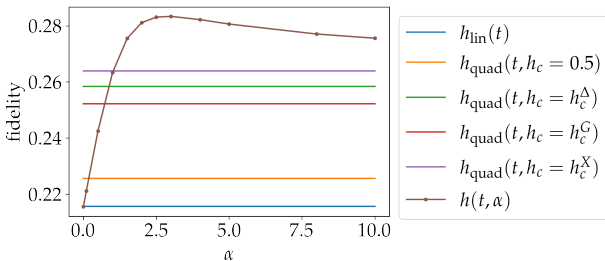


Figure 11: Final fidelity as a function of α for a single instance. The diagonal of the respective Hamiltonian \hat{H}_p , see Eq. (2), is provided in the supplemental material with the label B1.

4 Summary and Outlook

We have investigated the annealing and quench dynamics of a spin model incorporating the exact cover problem. While the quench dynamics exhibits a jump of the dynamical quench parameters (DQP), the annealing dynamics undergoes an equilibrium transition between a paramagnetic and a glassy state. We have shown that the DQP can be used to determine the minimal

annealing gap of the system through multivariate regression, see Figs. 3 and 4. Moreover, by means of a one-layer neural network, it even becomes possible to fully predict the gap function of a given instance, based on the field dependence of the DQP, see Fig. 6.

These findings enable the optimized design of quantum adiabatic protocols with significantly enhanced performance. In the present article, we have presented a practical advantage by feeding annealing protocols with the information of the DQP, see Figs. 7 and 11. At least if one disregards the time for the quench experiments, this leads to a time-to-solution benefit in annealing algorithms which has not been achieved yet, e.g., with pausing [42, 43].

Our study suggests that the annealing gap and the DQP are related in spin glass systems. This enables to draw instance-specific information about the problem Hamiltonian and its energy spectrum in a transverse field from simple quench experiments. Specifically, the magnetization after a quench which is readily measured can reveal the energy gap of the system in a transverse field. Moreover, it would be interesting to find a relation between the dynamical quantum phase transition and the annealing gap in the thermodynamic limit. This, however, requires a proper scaling of the system size which is not trivial to perform for random Hamiltonians. In this context, we have also given an example how modern machine learning algorithms can be used to support quantum annealing protocols and thus enhance their efficiency.

This new insight into the annealing gap is expected to trigger further research on optimal annealing protocols and the adiabatic theorem. We already have explicitly demonstrated that partial or full knowledge of the annealing gap can be used to improve the protocol, but as our simulation of the protocol defined in Eq. (17) has shown, simple adiabatic theorems are not sufficient to determine the *optimal* protocol.

Acknowledgments

The authors are grateful for enlightening discussions with Gabriel Fernández Fernández, Alexandre Dauphin, and Maciej Lewenstein. The authors acknowledge funding from “la Caixa” Foundation (ID 100010434, fellowship

code LCF/BQ/PI19/11690013), ERC AdG NOQIA, Spanish Ministry MINECO and State Research Agency AEI (FIDEUA PID2019-106901GB-I00/10.13039 / 501100011033, SEVERO OCHOA No. SEV-2015-0522 and CEX2019-000910-S, FPI), European Social Fund, Fundacio Cellex, Fundacio Mir-Puig, Generalitat de Catalunya (AGAUR Grant No. 2017 SGR 1341, CERCA program, QuantumCAT U16-011424, co-funded by ERDF Operational Program of Catalonia 2014-2020), MINECO-EU QUANTERA MAQS (funded by State Research Agency (AEI) PCI2019-111828-2 / 10.13039/501100011033), EU Horizon 2020 FET-OPEN OPTOLogic (Grant No 899794), and the National Science Centre, Poland-Symfonia Grant No. 2016/20/W/ST4/00314.

References

[1] M. H. S. Amin and V. Choi. First-order quantum phase transition in adiabatic quantum computation. *Phys. Rev. A*, 80:062326, Dec 2009. DOI: 10.1103/PhysRevA.80.062326. URL <https://link.aps.org/doi/10.1103/PhysRevA.80.062326>.

[2] Tameem Albash and Daniel A. Lidar. Adiabatic quantum computation. *Reviews of Modern Physics*, 90(1):015002, jan 2018. DOI: 10.1103/revmodphys.90.015002.

[3] Philipp Hauke, Helmut G Katzgraber, Wolfgang Lechner, Hidetoshi Nishimori, and William D Oliver. Perspectives of quantum annealing: methods and implementations. *Reports on Progress in Physics*, 83(5):054401, may 2020. DOI: 10.1088/1361-6633/ab85b8.

[4] M. Lewenstein, A. Sanpera, and V. Ahufinger. *Ultracold Atoms in Optical Lattices: Simulating Quantum Many-body Systems*. OUP Oxford, 2012. ISBN 9780199573127. URL <http://books.google.es/books?id=WX4Xz7F6DdUC>.

[5] R. Blatt and C. F. Roos. Quantum simulations with trapped ions. *Nature Physics*, 8(4):277–284, Apr 2012. ISSN 1745-2481. DOI: 10.1038/nphys2252. URL <https://doi.org/10.1038/nphys2252>.

[6] Alán Aspuru-Guzik and Philip Walther. Photonic quantum simulators. *Nature Physics*, 8(4):285–291, Apr 2012. ISSN 1745-2481. DOI: 10.1038/nphys2253. URL <https://doi.org/10.1038/nphys2253>.

[7] John Preskill. Quantum Computing in the NISQ era and beyond. *Quantum*, 2:79, August 2018. ISSN 2521-327X. DOI: 10.22331/q-2018-08-06-79. URL <https://doi.org/10.22331/q-2018-08-06-79>.

[8] F Barahona. On the computational complexity of Ising spin glass models. *J. Phys. A*, 15(10):3241, 1982. URL <http://stacks.iop.org/0305-4470/15/i=10/a=028>.

[9] M. W. Johnson, M. H. S. Amin, S. Gildert, T. Lanting, F. Hamze, N. Dickson, R. Harris, A. J. Berkley, J. Johansson, P. Bunyk, E. M. Chapple, C. Enderud, J. P. Hilton, K. Karimi, E. Ladizinsky, N. Ladizinsky, T. Oh, I. Perminov, C. Rich, M. C. Thom, E. Tolkacheva, C. J. S. Truncik, S. Uchaikin, J. Wang, B. Wilson, and G. Rose. Quantum annealing with manufactured spins. *Nature*, 473(7346):194–198, may 2011. ISSN 0028-0836. DOI: 10.1038/nature10012. URL <http://www.nature.com/nature/journal/v473/n7346/abs/10.1038-nature10012-unlocked.html#supplementary-information>.

[10] Philipp Hauke, Lars Bonnes, Markus Heyl, and Wolfgang Lechner. Probing entanglement in adiabatic quantum optimization with trapped ions. *Front. Phys.*, 3:21, 2015. ISSN 2296-424X. DOI: 10.3389/fphy.2015.00021. URL <http://journal.frontiersin.org/article/10.3389/fphy.2015.00021>.

[11] Tobias Graß, David Raventós, Bruno Juliá-Díaz, Christian Gogolin, and Maciej Lewenstein. Quantum annealing for the number-partitioning problem using a tunable spin glass of ions. *Nat. Commun.*, 7:11524, may 2016. DOI: 10.1038/ncomms11524;:::;:::;:::;:::;10.1038/ncomms11524.

[12] A. W. Glaetzle, R. M. W. van Bijnen, P. Zoller, and W. Lechner. A coherent quantum annealer with Rydberg atoms. *Nat. Commun.*, 8:15813, jun 2017. DOI: 10.1038/ncomms15813;:::;10.1038/ncomms15813. URL <https://www.nature.com/articles/ncomms15813#supplementary-information>.

[13] Valentin Torggler, Sebastian Krämer, and Helmut Ritsch. Quantum annealing

with ultracold atoms in a multimode optical resonator. *Phys. Rev. A*, 95:032310, Mar 2017. DOI: 10.1103/PhysRevA.95.032310. URL <https://link.aps.org/doi/10.1103/PhysRevA.95.032310>.

[14] Xingze Qiu, Peter Zoller, and Xiaopeng Li. Programmable quantum annealing architectures with ising quantum wires. *PRX Quantum*, 1:020311, Nov 2020. DOI: 10.1103/PRXQuantum.1.020311. URL <https://link.aps.org/doi/10.1103/PRXQuantum.1.020311>.

[15] E. Farhi, J. Goldstone, S. Gutmann, J. Lapan, A. Lundgren, and D. Preda. A quantum adiabatic evolution algorithm applied to random instances of an NP-complete problem. *Science*, 292(5516):472–475, apr 2001. DOI: 10.1126/science.1057726.

[16] Tadashi Kadowaki and Hidetoshi Nishimori. Quantum annealing in the transverse ising model. *Physical Review E*, 58(5):5355–5363, nov 1998. DOI: 10.1103/physreve.58.5355.

[17] J. Brooke, D. Bitko, F. T. Rosenbaum, and G. Aeppli. Quantum annealing of a disordered magnet. *Science*, 284(5415):779–781, 1999. DOI: 10.1126/science.284.5415.779. URL <https://science.sciencemag.org/content/284/5415/779>.

[18] Thomas Jörg, Florent Krzakala, Jorge Kurchan, and A. C. Maggs. Simple Glass Models and Their Quantum Annealing. *Phys. Rev. Lett.*, 101:147204, Oct 2008. DOI: 10.1103/PhysRevLett.101.147204. URL <https://link.aps.org/doi/10.1103/PhysRevLett.101.147204>.

[19] A. P. Young, S. Knysh, and V. N. Smelyanskiy. First-Order Phase Transition in the Quantum Adiabatic Algorithm. *Phys. Rev. Lett.*, 104:020502, Jan 2010. DOI: 10.1103/PhysRevLett.104.020502. URL <https://link.aps.org/doi/10.1103/PhysRevLett.104.020502>.

[20] Thomas Jörg, Florent Krzakala, Guillehem Semerjian, and Francesco Zamponi. First-Order Transitions and the Performance of Quantum Algorithms in Random Optimization Problems. *Phys. Rev. Lett.*, 104:207206, May 2010. DOI: 10.1103/PhysRevLett.104.207206. URL <https://link.aps.org/doi/10.1103/PhysRevLett.104.207206>.

[21] Boris Altshuler, Hari Krovi, and Jérémie Roland. Anderson localization makes adiabatic quantum optimization fail. *Proc. Nat. Acad. Sci. USA*, 107(28):12446–12450, 2010. DOI: 10.1073/pnas.1002116107. URL <http://www.pnas.org/content/107/28/12446.abstract>.

[22] Sergey Knysh. Zero-temperature quantum annealing bottlenecks in the spin-glass phase. *Nat. Commun.*, 7(1):12370, Aug 2016. DOI: 10.1038/ncomms12370. URL <https://doi.org/10.1038/ncomms12370>.

[23] Neil G. Dickson and M. H. S. Amin. Does Adiabatic Quantum Optimization Fail for NP-Complete Problems? *Phys. Rev. Lett.*, 106:050502, Feb 2011. DOI: 10.1103/PhysRevLett.106.050502. URL <https://link.aps.org/doi/10.1103/PhysRevLett.106.050502>.

[24] Edward Farhi, Jeffrey Goldstone, David Gosset, Sam Gutmann, Harvey B. Meyer, and Peter Shor. Quantum adiabatic algorithms, small gaps, and different paths. *Quant. Inf. Comput.*, 11:181, 2011.

[25] Neil G. Dickson and Mohammad H. Amin. Algorithmic approach to adiabatic quantum optimization. *Phys. Rev. A*, 85:032303, Mar 2012. DOI: 10.1103/PhysRevA.85.032303. URL <https://link.aps.org/doi/10.1103/PhysRevA.85.032303>.

[26] Trevor Lanting, Andrew D. King, Bram Evert, and Emile Hoskinson. Experimental demonstration of perturbative anticrossing mitigation using nonuniform driver Hamiltonians. *Phys. Rev. A*, 96:042322, Oct 2017. DOI: 10.1103/PhysRevA.96.042322. URL <https://link.aps.org/doi/10.1103/PhysRevA.96.042322>.

[27] Yuya Seki and Hidetoshi Nishimori. Quantum annealing with antiferromagnetic fluctuations. *Phys. Rev. E*, 85:051112, May 2012. DOI: 10.1103/PhysRevE.85.051112. URL <https://link.aps.org/doi/10.1103/PhysRevE.85.051112>.

[28] Elizabeth Crosson, Edward Farhi, Cedric Yen-Yu Lin, Han-Hsuan Lin, and Peter Shor. Different strategies for optimization using the quantum adiabatic algorithm, 2014.

[29] Layla Hormozi, Ethan W. Brown, Giuseppe Carleo, and Matthias Troyer. Nonstoquastic Hamiltonians and quantum annealing

of an Ising spin glass. *Phys. Rev. B*, 95:184416, May 2017. DOI: 10.1103/PhysRevB.95.184416. URL <https://link.aps.org/doi/10.1103/PhysRevB.95.184416>.

[30] Tameem Albash. Role of nonstoquastic catalysts in quantum adiabatic optimization. *Phys. Rev. A*, 99:042334, Apr 2019. DOI: 10.1103/PhysRevA.99.042334. URL <https://link.aps.org/doi/10.1103/PhysRevA.99.042334>.

[31] I. Ozfidan *et al.* Demonstration of nonstoquastic Hamiltonian in coupled superconducting flux qubits. *arXiv 1903.06139*, 2019.

[32] Alejandro Perdomo-Ortiz, Salvador E. Venegas-Andraca, and Alán Aspuru-Guzik. A study of heuristic guesses for adiabatic quantum computation. *Quantum Information Processing*, 10(1):33–52, Feb 2011. ISSN 1573-1332. DOI: 10.1007/s11128-010-0168-z. URL <https://doi.org/10.1007/s11128-010-0168-z>.

[33] Masaki Ohkuwa, Hidetoshi Nishimori, and Daniel A. Lidar. Reverse annealing for the fully connected p -spin model. *Phys. Rev. A*, 98:022314, Aug 2018. DOI: 10.1103/PhysRevA.98.022314. URL <https://link.aps.org/doi/10.1103/PhysRevA.98.022314>.

[34] C. L. Baldwin and C. R. Laumann. Quantum algorithm for energy matching in hard optimization problems. *Phys. Rev. B*, 97:224201, Jun 2018. DOI: 10.1103/PhysRevB.97.224201. URL <https://link.aps.org/doi/10.1103/PhysRevB.97.224201>.

[35] Tobias Graß. Quantum annealing with longitudinal bias fields. *Phys. Rev. Lett.*, 123:120501, Sep 2019. DOI: 10.1103/PhysRevLett.123.120501. URL <https://link.aps.org/doi/10.1103/PhysRevLett.123.120501>.

[36] Zhijie Tang and Eliot Kapit. Unconventional quantum annealing methods for difficult trial problems. *Phys. Rev. A*, 103:032612, Mar 2021. DOI: 10.1103/PhysRevA.103.032612. URL <https://link.aps.org/doi/10.1103/PhysRevA.103.032612>.

[37] Nicholas Chancellor. Modernizing quantum annealing using local searches. *New J. Phys.*, 19(2):023024, feb 2017. DOI: 10.1088/1367-2630/aa59c4.

[38] Tobias Graß and Maciej Lewenstein. Hybrid annealing: Coupling a quantum simulator to a classical computer. *Phys. Rev. A*, 95:052309, May 2017. DOI: 10.1103/PhysRevA.95.052309. URL <https://link.aps.org/doi/10.1103/PhysRevA.95.052309>.

[39] James G. Morley, Nicholas Chancellor, Sougato Bose, and Viv Kendon. Quantum search with hybrid adiabatic–quantum-walk algorithms and realistic noise. *Phys. Rev. A*, 99:022339, Feb 2019. DOI: 10.1103/PhysRevA.99.022339. URL <https://link.aps.org/doi/10.1103/PhysRevA.99.022339>.

[40] Adam Callison, Nicholas Chancellor, Florian Mintert, and Viv Kendon. Finding spin glass ground states using quantum walks. *New Journal of Physics*, 21(12):123022, dec 2019. DOI: 10.1088/1367-2630/ab5ca2. URL <https://doi.org/10.1088/1367-2630/ab5ca2>.

[41] Jérémie Roland and Nicolas J. Cerf. Quantum search by local adiabatic evolution. *Physical Review A*, 65(4):042308, mar 2002. DOI: 10.1103/physreva.65.042308.

[42] Jeffrey Marshall, Davide Venturelli, Itay Hen, and Eleanor G. Rieffel. Power of pausing: Advancing understanding of thermalization in experimental quantum annealers. *Physical Review Applied*, 11(4):044083, apr 2019. DOI: 10.1103/physrevapplied.11.044083.

[43] Huo Chen and Daniel A. Lidar. Why and when pausing is beneficial in quantum annealing. *Physical Review Applied*, 14(1):014100, jul 2020. DOI: 10.1103/physrevapplied.14.014100.

[44] Adam Callison, Max Festenstein, Jie Chen, Laurentiu Nita, Viv Kendon, and Nicholas Chancellor. Energetic perspective on rapid quenches in quantum annealing. *PRX Quantum*, 2:010338, Mar 2021. DOI: 10.1103/PRXQuantum.2.010338. URL <https://link.aps.org/doi/10.1103/PRXQuantum.2.010338>.

[45] Lucas T. Brady, Christopher L. Baldwin, Aniruddha Bapat, Yaroslav Kharkov, and Alexey V. Gorshkov. Optimal protocols in quantum annealing and quantum approximate optimization algorithm problems. *Phys. Rev. Lett.*, 126:070505, Feb 2021. DOI: 10.1103/PhysRevLett.126.070505. URL <https://link.aps.org/doi/10.1103/PhysRevLett.126.070505>.

[46] Emil A. Yuzbashyan, Oleksandr Tsyplyatyev, and Boris L. Altshuler. Relaxation and persistent oscillations of the order parameter in fermionic condensates. *Phys. Rev. Lett.*, 96:097005, Mar 2006. DOI: 10.1103/PhysRevLett.96.097005. URL <https://link.aps.org/doi/10.1103/PhysRevLett.96.097005>.

[47] Bruno Scialla and Giulio Biroli. Quantum quenches and off-equilibrium dynamical transition in the infinite-dimensional bose-hubbard model. *Phys. Rev. Lett.*, 105:220401, Nov 2010. DOI: 10.1103/PhysRevLett.105.220401. URL <https://link.aps.org/doi/10.1103/PhysRevLett.105.220401>.

[48] Jad C. Halimeh, Valentin Zauner-Stauber, Ian P. McCulloch, Inés de Vega, Ulrich Schollwöck, and Michael Kastner. Prethermalization and persistent order in the absence of a thermal phase transition. *Phys. Rev. B*, 95:024302, Jan 2017. DOI: 10.1103/PhysRevB.95.024302. URL <https://link.aps.org/doi/10.1103/PhysRevB.95.024302>.

[49] Jad C. Halimeh and Valentin Zauner-Stauber. Dynamical phase diagram of quantum spin chains with long-range interactions. *Phys. Rev. B*, 96:134427, Oct 2017. DOI: 10.1103/PhysRevB.96.134427. URL <https://link.aps.org/doi/10.1103/PhysRevB.96.134427>.

[50] Ingo Homrighausen, Nils O. Abeling, Valentin Zauner-Stauber, and Jad C. Halimeh. Anomalous dynamical phase in quantum spin chains with long-range interactions. *Phys. Rev. B*, 96:104436, Sep 2017. DOI: 10.1103/PhysRevB.96.104436. URL <https://link.aps.org/doi/10.1103/PhysRevB.96.104436>.

[51] Bojan Žunkovič, Markus Heyl, Michael Knap, and Alessandro Silva. Dynamical quantum phase transitions in spin chains with long-range interactions: Merging different concepts of nonequilibrium criticality. *Physical Review Letters*, 120(13):130601, mar 2018. DOI: 10.1103/physrevlett.120.130601.

[52] R. Jafari. Dynamical quantum phase transition and quasi particle excitation. *Scientific Reports*, 9(1), feb 2019. DOI: 10.1038/s41598-019-39595-3.

[53] Utkarsh Mishra, R Jafari, and Alireza Akbari. Disordered kitaev chain with long-range pairing: Loschmidt echo revivals and dynamical phase transitions. *Journal of Physics A: Mathematical and Theoretical*, 53(37):375301, aug 2020. DOI: 10.1088/1751-8121/ab97de.

[54] J. Zhang, G. Pagano, P. W. Hess, A. Kyprianidis, P. Becker, H. Kaplan, A. V. Gorshkov, Z.-X. Gong, and C. Monroe. Observation of a many-body dynamical phase transition with a 53-qubit quantum simulator. *Nature*, 551(7682):601–604, Nov 2017. ISSN 1476-4687. DOI: 10.1038/nature24654. URL <https://doi.org/10.1038/nature24654>.

[55] Marin Bukov, Alexandre G. R. Day, Dries Sels, Phillip Weinberg, Anatoli Polkovnikov, and Pankaj Mehta. Reinforcement learning in different phases of quantum control. *Phys. Rev. X*, 8: 031086, Sep 2018. DOI: 10.1103/PhysRevX.8.031086. URL <https://link.aps.org/doi/10.1103/PhysRevX.8.031086>.

[56] Jian Lin, Zhong Yuan Lai, and Xiaopeng Li. Quantum adiabatic algorithm design using reinforcement learning. *Phys. Rev. A*, 101:052327, May 2020. DOI: 10.1103/PhysRevA.101.052327. URL <https://link.aps.org/doi/10.1103/PhysRevA.101.052327>.

[57] Phillip Weinberg and Marin Bukov. QuSpin: a python package for dynamics and exact diagonalisation of quantum many body systems part i: spin chains. *SciPost Physics*, 2(1), feb 2017. DOI: 10.21468/scipostphys.2.1.003.

[58] Phillip Weinberg and Marin Bukov. QuSpin: a python package for dynamics and exact diagonalisation of quantum many body systems. part II: bosons, fermions and higher spins. *SciPost Physics*, 7(2), aug 2019. DOI: 10.21468/scipostphys.7.2.020.

[59] Pankaj Mehta, Marin Bukov, Ching-Hao Wang, Alexandre G.R. Day, Clint Richardson, Charles K. Fisher, and David J. Schwab. A high-bias, low-variance introduction to machine learning for physicists. *Physics Reports*, 810:1–124, may 2019. DOI: 10.1016/j.physrep.2019.03.001.

[60] François Chollet et al. Keras. <https://keras.io>, 2015.